SOFT ROBOTS

Multimodal soft valve enables physical responsiveness for preemptive resilience of soft robots

Marco Pontin[1,2]* and Dana D. Damian[1,2,3]*

Copyright © 2024 The Authors, some rights reserved; exclusive licensee American Association for the Advancement of Science. No claim to original U.S. Government Works

Resilience is crucial for the self-preservation of biological systems: Humans recover from wounds thanks to an immune system that autonomously enacts a multistage response to promote healing. Similar passive mechanisms can enable pneumatic soft robots to overcome common faults such as bursts originating from punctures or overpressurization. Recent technological advancements, ranging from fault-tolerant controllers for robot reconfigurability to self-healing materials, have paved the way for robot resilience. However, these techniques require powerful processors and large datasets or external hardware. How to extend the operational life span of damaged soft robots with minimal computational and physical resources remains unclear. In this study, we demonstrated a multimodal pneumatic soft valve capable of passive resilient reactions, triggered by faults, to prevent or isolate damage in soft robots. In its forward operation mode, the valve, requiring a single supply pressure, isolated punctured soft inflatable elements from the rest of the soft robot in as fast as 21 milliseconds. In its reverse operation mode, the valve can passively protect robots against overpressurization caused by external disturbances, avoiding plastic deformations and bursts. Furthermore, the two modes combined enabled the creation of an endogenously controlled valve capable of autonomous burst isolation. We demonstrated the passive and quick response and the possibility of monolithic integration of the soft valve in grippers and crawling robots. The approach proposed in this study provides a distributed small-footprint alternative to controller-based resilience and is expected to help soft robots achieve uninterrupted long-lasting operation.

INTRODUCTION

Soft robots demonstrate advanced capabilities such as high deformation, inherent shock absorbance, and light structures compared with those of classical rigid robots because of the compliance of their bodies. Hence, they are promising for applications in human-robot interaction, medical robots, and marine and space robots (*1*–*7*). Most soft robots are fluidically actuated because such systems entail reduced complexity in fabrication and integration. In particular, pneumatic actuators, which consist of one or more chambers, are connected to a pressure input to enable pressurization and, consequently, robotic motion. In addition, electromechanical components such as valves and control logic and pressure sensors are required for pressure regulation.

Despite their promising potential, fluidic soft robots are prone to failure just as much as traditional robots. Bursts from cuts or overpressurization represent a common and critical mode of failure, which leads to unresponsive robots and reduces their reliability and potential for adoption (*8*, *9*). Vulnerabilities in technologies are a well-known challenge, with recognized unfavorable economic consequences and risks to humans. The classical fault-tolerant framework (*10*) built around rigid machines relies on complex control algorithms to achieve behavior adaptation after a critical fault to salvage as much capability of the system as possible (*11*, *12*). In the same framework, reconfigurable and self-assembling systems have been researched to grant spare parts to robots in cases of breakages (*13*–*15*). However, these approaches assume discrete, addressable points of failure such as sensors, actuators, or links, making it difficult to scale these techniques to high–degree-of-freedom machines or the entire body of a robot. In addition, the entire framework is based on a centralized architecture in which the controller makes decisions on the basis of feedback from various sensors, often requiring precise models or extensive training, which is usually computationally demanding.

Soft robots introduced an embodied approach to fault recovery with self-healing materials, which exploit chemically enabled repairs (such as reversible Diels-Alder bonds and hydrogen bonds). This approach is highly distributed and does not require a model or extensive computations (*8*, *16*–*21*). Although self-healing materials are fundamental to soft robotic resilience, they suffer from some limitations. For example, the healing can be time-consuming, and external stimuli or human intervention is sometimes required to complete the healing process. Furthermore, fluidic actuators must remain deflated to their neutral state for the healing to occur, and, if part of the material is removed during the fault, the chances of recovery are diminished markedly.

Resilience in living creatures shows a level of nuance that robots continue to lack. For instance, humans benefit from a multistage process to treat injuries, activated by the innate immune system. A wounded finger triggers a tightly coordinated cascade of reactions at different time scales (*22*–*24*). First, a local inflammatory response is generated to prevent blood loss and protect against infection. In the medium term, growth factors are released, triggering cell proliferation and skin regeneration. Although these reactions take place passively and unconsciously, humans adopt cautious behaviors meant to aid in the recovery of the injured finger. Therefore, biological organisms inspire developing responsive resilience strategies for autonomous fault isolation so that damage does not propagate further and the system remains operational until full recovery is achieved through methods such as material-level healing. Soft matter–embodied mechanisms that can react to a fault instantly and passively, to stop further harm to the robot or its environment, are therefore needed; however, this remains an unexplored area. Valves, which constitute fundamental computational elements in fluidic systems, could be used for such purposes.

[1]Department of Automatic Control and Systems Engineering, University of Sheffield, Sheffield, UK. [2]Sheffield Robotics, University of Sheffield, Sheffield, UK. [3]Insigneo Institute for In Silico Medicine, University of Sheffield, Sheffield, UK.
*Corresponding author. Email: mpontin1@sheffield.ac.uk (M.P.); d.damian@sheffield.ac.uk (D.D.)

Downloaded from https://www.science.org at The Hong Kong University of Science and Technology (Guangzhou) on May 25, 2026

Soft valves have evolved considerably, fueled by research into realizing soft matter digital and analog fluidic components to control soft robots. Microfluidic research has demonstrated the possibility of replicating complex digital logic circuits (*25*–*27*) while achieving compact designs (*28*). In addition, recent advancements in three-dimensional (3D) printing techniques and materials have permitted the merging of control logic and actuators into one unit, leading to the creation of monolithic soft robots (*29*–*31*), thus decreasing their production costs and time. Recent work showing soft matter valves, pumps, and controllers has demonstrated the possibility of creating entirely soft robots (*32*–*35*). In particular, the development of valves, guided by the parallels between fluidic and electric system modeling (*36*), targets the replication of functionalities obtained with complementary metal-oxide semiconductor (CMOS) technologies for logic and computational purposes (*37*, *38*). Other soft matter valve designs have exploited mechanical phenomena such as bistability (*39*, *40*) and buckling (*41*) to create oscillators for robot control and locomotion (*42*). Furthermore, the combination of state-of-the-art inkjet printing and monopropellant fluids (*43*) has led to the development of soft robots that include fluidic controllers and onboard pressure generation (*29*). Despite these advancements in replicating complex behaviors through ingenious fluidic circuits, using such circuits for soft robot resilience assumes that the robot is equipped with pressure sensors and valves for every functional fluidic chamber, centralized control, and a quick response time. All of these factors increase the hardware and computational burdens.

The use of soft valves to endow robots with matter-embedded responsive resilience is a recent, understudied development. In (*44*), our group designed and characterized a valve that can automatically detect bursts and perform isolation, whereas in (*45*), a soft-fuse valve for realizing the same purpose was proposed. Here, inspired by the passive and autonomous nature of mechanisms observed in living beings, we present a fully soft valve that exhibited multimodal behavior to achieve passive distributed resilience in pneumatic soft robots. The passive autonomous burst detection and isolation behavior was triggered in the forward operation mode (FOM) of the soft valve, whereas in the reverse operation mode (ROM), the soft valve passively detected and protected against the overpressurization of the actuators. In both cases, the valve exploited pressure differences induced by the faults to trigger its own response, either preventing the failure or avoiding its propagation to the system. Last, the multimodality of the valve was used to create an endogenously controlled (EC) two-stage soft valve that can generate its own control signal, avoiding the need for an externally actuated line while maintaining burst detection and isolation capabilities. The resilient capabilities enabled by the multimodal soft valve were exhibited in several manipulation and locomotion demonstrations. The innovations in this study demonstrate embodied fluidic circuits that preemptively responded to damages in soft robots, thus extending their operational life span with minimal resources and facilitating the development of an embodied unified platform for bioinspired treatment of malfunctions.

RESULTS

Design and working principles of the soft valve

The pneumatic soft valve, shown in Fig. 1A, consists of three functional layers. The membrane separates the control layer, where the control chamber resides, from the flow layer, which connects the main inlet and outlet ports. The integrated tubing in the valve acts as a constraint, preventing the associated section of the channel from expanding when pressurized, and serves as a localized resistance for the airflow. The single-material design and compact structure enable simple integration into existing soft robots. The geometry and position of the internal channels were selected to grant multimodality, that is, different operation modes depending on how the valve is connected to a soft actuator, with a single supply pressure. In particular, we distinguish between an FOM and an ROM.

In FOM, the narrow vertical channel serves as the inlet (Fig. 1B). When a sufficiently high-pressure difference is reached between the control pressure p_c and outlet pressure p_{out} ($\boldsymbol{p_c > p_{out}}$), the membrane deforms and obstructs the inlet channel, thereby separating the inlet from the outlet (closed condition). In this mode, the valve can be considered the fluidic equivalent of a resettable fuse. If the valve's outlet is paired with a soft inflatable element (SIE), such as a pneumatic actuator or sensor, then passive autonomous burst detection and isolation can be achieved. The burst causes the pressure level underneath the membrane to drop suddenly, leading the membrane to deform downward and obstruct the inlet channel, isolating the faulty SIE from the rest of the system. Instrumental in achieving this result is the high impedance of the inlet channel, which decouples the inlet and outlet pressures (fig. S1).

In ROM, the narrow channel serves as the outlet, as shown in Fig. 1C. The valve starts out closed and later opens when the pressure difference between the chambers on either side of the membrane, $p_c - p_{in}$, drops below a threshold value Δp_{th} dependent on the geometry and material properties of the valve. Under these conditions, the deformed membrane no longer obstructs the outlet channel, and air can discharge through the valve. In this mode, the valve acts as the equivalent of a Zener diode and, as such, if the valve's inlet is connected to an SIE, then it can be used to protect the valve against overpressurization events.

Multimodality is achieved because of the asymmetric geometry of the valve. The control pressure acts on the same surface of the membrane, independent of the operating mode. In contrast, the inlet pressure acts on different areas, depending on the mode. In FOM, when the valve is closed, the area is equal to that of the inlet channel tubing, so the valve can remain closed, even when the inlet and control pressures are equal. In ROM, the pressure acts on the side area of the deformed membrane that is not in contact with the bottom of the flow layer chamber. This change in the active area causes the valve to open, even when p_{in} is lower than p_c. This multimodality enables the creation of an EC soft valve capable of self-tuning operation. By combining two soft valves in a two-stage stacked assembly, this version of the soft valve can generate its own control signal, adapting to the inflation transient of the SIE it is paired to. Consequently, passive burst detection and isolation functionality are achieved without an external control line being present.

Soft valve provides resilience against bursts

Forward operation mode characterization

In FOM, the valve is positioned between the main pressure source and the SIE, and it requires two external signals, inlet and control, at the same supply pressure level, p_s, for operation (Fig. 2A). A representative burst detection and isolation experiment used to characterize the valve's response time (see Materials and Methods for details) is presented in Fig. 2B. The flow layer was pressurized first, followed by the control layer. Because the same pressure, p_s, acted on both sides of the

Downloaded from https://www.science.org at The Hong Kong University of Science and Technology (Guangzhou) on May 25, 2026

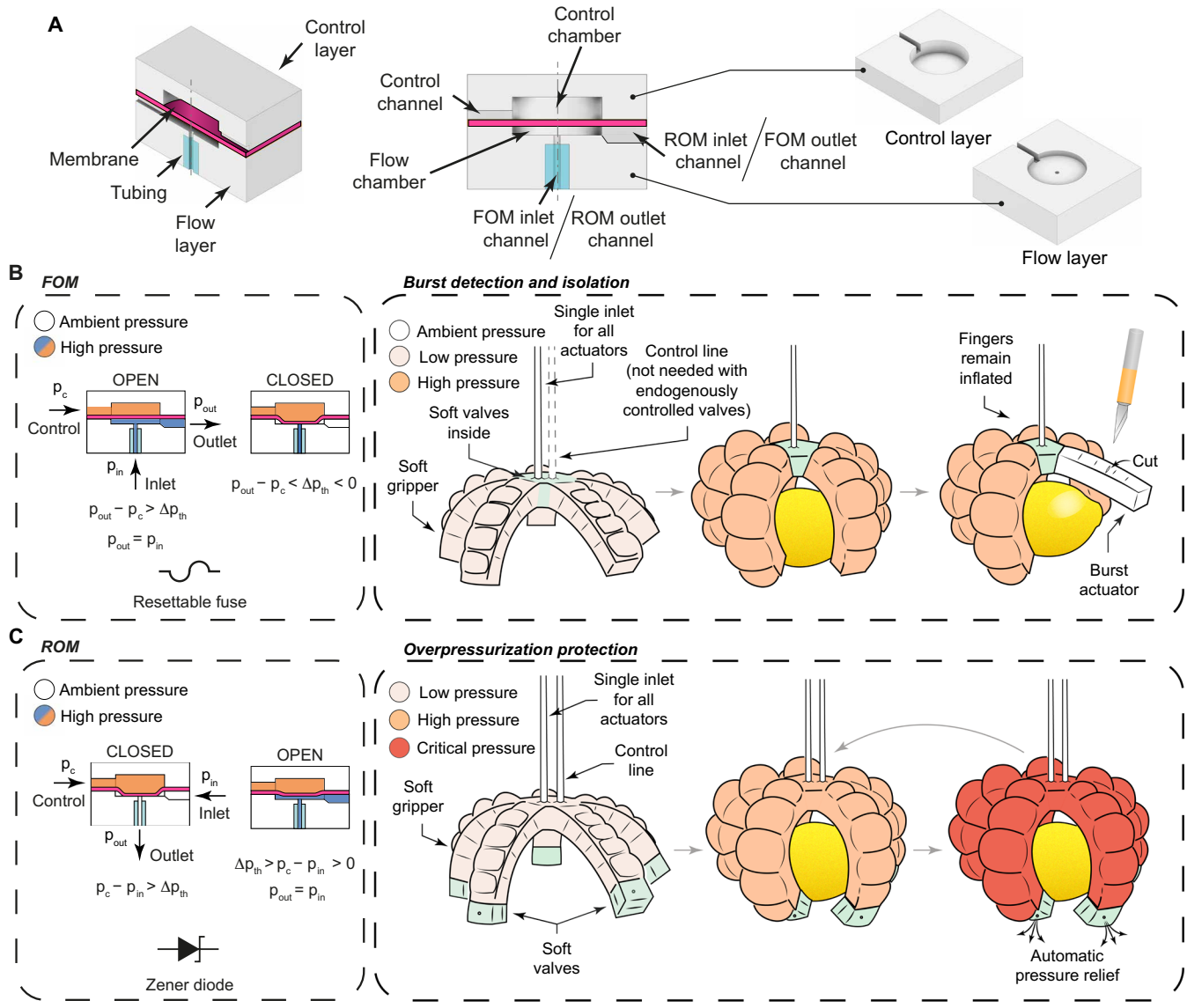

Fig. 1. Details of the soft valve and possible applications. (**A**) Internal structure of the valve and its main components. (**B**) The soft valve, configured in FOM, can act as a resettable fuse. When paired with soft actuators, the valve can automatically detect and isolate bursts, preventing a single actuator fault from affecting the whole system. (**C**) The ROM turns the valve into the equivalent of a Zener diode. In this configuration, the valve can protect actuators against damage from overpressurization caused either by controller error or by external disturbances.

membrane, the valve remained open for further inflation of the SIE. When a burst occurred ($t = 4.0$ s), the pressure underneath the membrane dropped quickly because of the asymmetric distribution of the internal fluidic resistances, causing the membrane to deform, obstruct the inlet, and isolate the outlet. The pressure difference between the two sides of the membrane depends on the ratio of the inlet to the outlet resistance within the soft valve (fig. S2). After the burst, the equilibrium equation for the membrane can be written as

$$\frac{\pi}{4}\left[p_c\left(D^2 - d_c^{\,2}\right) - d^2\left(p_c - p_{in}\right)\right] - fm = 0 \qquad (1)$$

where D, d, d_c, and fm represent the membrane diameter (Fig. 2C and fig. S3), the inlet channel diameter, the diameter of the contact area between the membrane and the bottom of the flow layer chamber, and the elastic force associated with the deformed membrane, respectively. After the burst, the valve remained closed until the control signal was removed.

The valve requires a quick response time and sufficient input impedance to operate correctly for burst isolation. To understand the effects of the internal geometry of the valve, we investigated how the membrane thickness, h, and both diameters, d and D, affect the switching time, Δt. For the range that was tested, the membrane thickness did not alter the performance in a significant manner [average P value of analysis of variance (ANOVA) was $P = 0.22$; table S1], with all valves averaging a switching time of 25.11 ms (SD = 1.99 ms) (Fig. 2D). More pronounced changes were observed when comparing the different internal geometries. As expected, narrower inlet channels led to faster switching times because of higher input impedance. The largest channel ($d = 1.5$ mm)

Downloaded from https://www.science.org at The Hong Kong University of Science and Technology (Guangzhou) on May 25, 2026

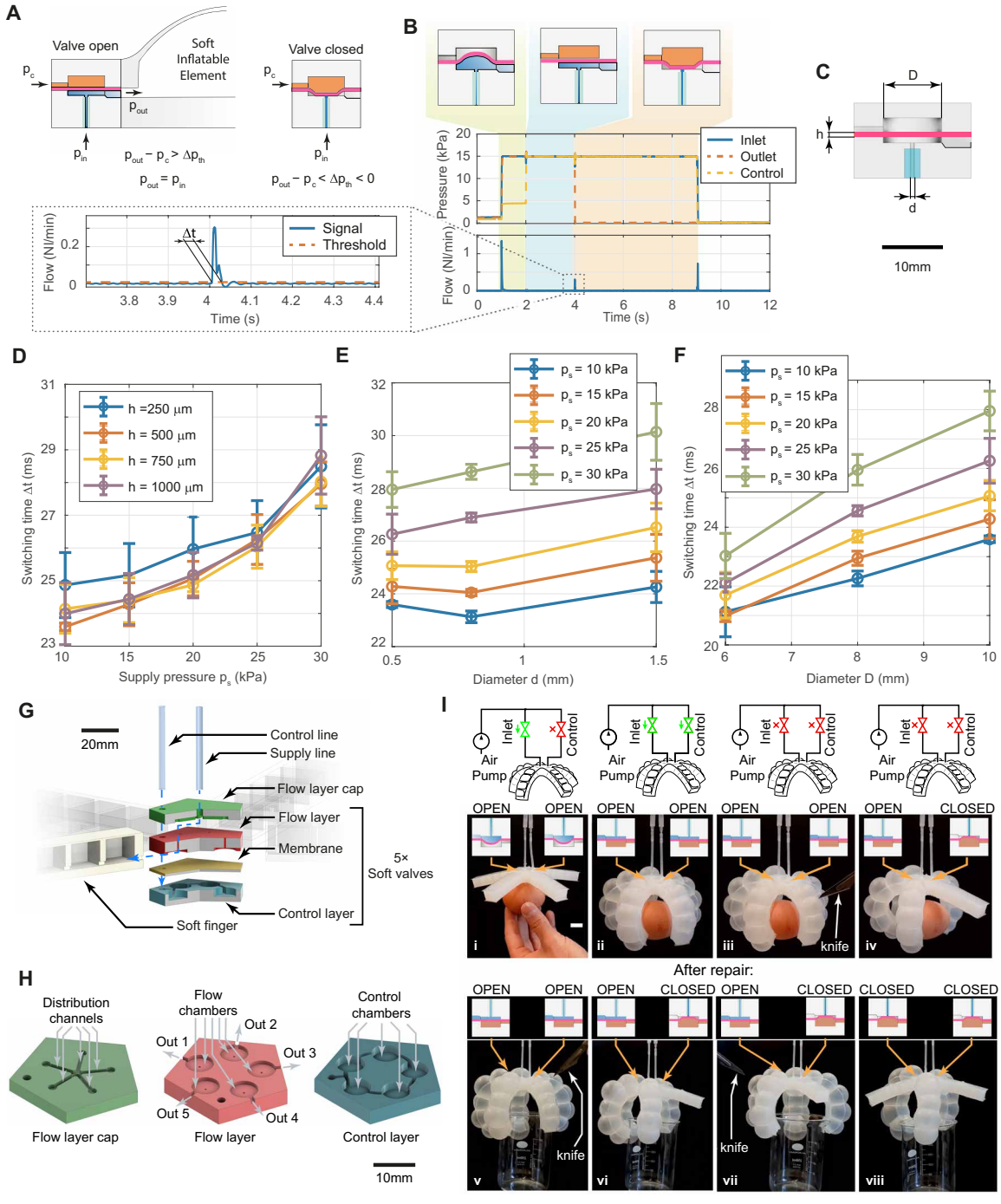

Fig. 2. FOM behavior characterization and demonstration. (**A**) Working principle of the FOM. (**B**) Example experiment used to evaluate the valve's reaction time upon a simulated burst ($D = 10$ mm, $d = 0.5$ mm, and $h = 500$ μm). The beginning and end of the flow rate spike are used to compute Δt. (**C**) Internal structure of the valve and relevant geometrical parameters. (**D**) Switching time of soft valves with different membrane thicknesses ($D = 10$ mm and $d = 0.5$ mm). Error bars in plots indicate the average SD ($N = 15$) obtained in the trials [also for (E) and (F)]. For details on statistical analysis, please refer to Materials and Methods. (**E**) Narrower inlet channels provide higher input impedance, leading to faster switching times ($D = 10$ mm, and $h = 500$ μm). (**F**) Smaller D and lower supply pressures translate into faster, more reactive valves ($d = 0.5$ mm, and $h = 500$ μm). (**G**) Internal structure of the five-finger soft gripper with integrated soft valves ($D = 6$ mm, $d = 0.5$ mm, and $h = 500$ μm). Only one supply and one control channel are needed to control the gripper and achieve the burst isolation capability, therefore limiting hardware requirements and control logic complexity. (**H**) Structure of the palm integrating the soft valves. (**I**) Demonstration of the burst detection and isolation capabilities. The scale bar in the figure represents 20 mm. First, the gripper was inflated and isolated from the supply (i and ii). One of the fingers was then burst with a precision knife (iii), but the gripper maintained its grasp on the egg it was holding because of the action of the soft valve connected to the finger (iv). The faulty finger was repaired using a thin layer of glue, and then the gripper was reinflated to grasp a glass beaker (v and vi). Two fingers were then burst while keeping the object suspended, showing that if more than one finger fails, the fault detection and isolation still work, independently for each finger (vii and viii).

Downloaded from https://www.science.org at The Hong Kong University of Science and Technology (Guangzhou) on May 25, 2026

averaged 27.1 ms across the supply pressure levels compared with 25.8 ms for the thinnest one (Fig. 2E). However, the largest change in performance was observed by decreasing the diameter D of the chamber (smaller, more reactive membrane) (Fig. 2F), with an average difference of 3.64 ms between the fastest ($D = 6$ mm) and slowest ($D = 10$ mm) geometries and an overall 17.6% improvement (at 30 kPa). Furthermore, the valve's operation under deformation was tested (Supplementary Methods and fig. S4): The valve operated reliably for up to 17% unidirectional compressive strain with a 1000-μm membrane or up to 25% strain with a 250-μm membrane. Last, the valve resumed its normal behavior as soon as the external load was removed. In terms of long-term reliability, lifetime experiments on three soft valves showed no noticeable change in performance after 5000 cycles (Supplementary Methods and fig. S5).

Burst detection and isolation in a five-finger pneumatic soft gripper

A five-finger elastomeric gripper was used to demonstrate the functionality of the valve in FOM. As shown in Fig. 2G, each finger consists of a Pneu-Net–type actuator (*46*) that bends upon inflation. The fingers are connected to a palm that incorporates one soft valve for each finger (Fig. 2H). All valves are configured in FOM, and only two inlets to the system are required, one for the inflation of the gripper and the other for the pressurization of the control channel, which are shared among all five valves.

The gripper was inflated to grasp an uncooked egg. The control channel was then pressurized, activating the burst detection and isolation functionality (Fig. 2I, i and ii, and movie S1). When one finger contacts a sharp object, it bursts suddenly, causing the corresponding soft valve to switch and isolate it from the other fingers. As a result, the remaining four fingers maintained their grasp on the object, preventing it from falling (Fig. 2I, iii and iv). The hole in the faulty finger was sealed using a thin layer of Sil-Poxy glue, and the gripper was reused to grasp a different object (Fig. 2Iv). This time, two fingers were punctured, yet the gripper maintained a firm grasp on the object (Fig. 2I, vi to viii), further proving the independence between the fingers.

Reversed soft valve protects against overpressurization

Reverse operation mode characterization

In ROM, the control channel starts out pressurized at pressure p_s, and the deformed membrane obstructs the narrow outlet channel (valve closed). The second external input is represented by the inlet channel supplied with the same p_s. Once the difference between p_c and p_{in} reaches a threshold value, Δp_{th}, the membrane can no longer obstruct the outlet, and the soft valve opens (Fig. 3A). Contrary to what occurs in FOM, in ROM, the equilibrium equation for the deformed membrane (fig. S3) is

$$\frac{\pi}{4}\left(p_c - p_{in}\right)\left(D^2 - {d_c}^2\right) - fm = 0 \quad (2)$$

The ROM behavior of the soft valve is experimentally captured in Fig. 3B. The control channel was pressurized and immediately reached the supply pressure value p_s. The inlet channel was then activated. As the inlet pressure increased, the outlet pressure remained at ambient pressure, indicating that the outlet was isolated from the inlet. When the condition $p_c - p_{in} < \Delta p_{th}$ was reached, the valve opened, and the outlet pressure p_{out} suddenly rose, matching the value of p_{in}. The stability of the valve near the threshold pressure difference was verified by checking for unintended autonomous switching of the soft valve (fig. S6).

Analysis of the effect of the membrane thickness and control pressure showed that, for the same control pressure, thicker membranes required lower values of p_{in} (larger Δp_{th}) for the valve to open (Fig. 3C). These results can be explained by the superposition of two effects. Thicker membranes deformed less at the same control pressure, leaving more side areas exposed to the effect of the inlet pressure p_{in}. The second effect is that of fm, which increased with membrane thickness and pressure p_c, lowering the threshold pressure required for the valve to open. A slight upward trend is present in the results, irrespective of the membrane thickness; however, the change in Δp_{th} was always less than 2.5 kPa. The downward slope observed in the percentage results, obtained as $\frac{\Delta p_{th}}{p_s}$, demonstrated that this increase was more than compensated for by the increase in the corresponding supply pressure. In addition, thinner membranes showed a more uniform, flattened performance across the various supply pressures: An overall change of 0.7 kPa in Δp_{th} was observed for the 250-μm membrane, whereas this increased to 2.4 kPa with a 750-μm-thick membrane.

The comparison of different internal geometries indicated that both diameters D and d affected the valve's performance (fig. S7); however, a change in D provided a larger variation. Figure 3D shows a comparison of all different geometries through the metric $D - d$ (chosen for improved visualization of the results): D is proportional to the contact diameter, d_c, of the membrane with the chamber, and d represents the critical value for d_c below which the valve is open. As shown in Fig. 3D, there seems to be an optimal value for $D - d$, equal to 8.5 mm with a 500-μm membrane, which minimizes both Δp_{th} for each supply pressure level and its variation across supply levels, thereby leading to an overall better performance of the ROM-configured valve.

Overpressurization protection in a pneumatic soft hand

The ROM-configured soft valve was embedded in an elastomeric two-finger hand to demonstrate the overpressurization protection capability (Fig. 3E and movie S2). Upon inflation, the fingers bend, making it possible to simulate a handshake for human-robot interaction scenarios. Only one finger had a ROM-configured soft valve at its tip ($D = 10$ mm, $d = 0.8$ mm, and membrane thickness $h = 500$ μm), making it possible to better highlight the effect of the valve on the behavior of the gripper. The soft valve's control chamber was pressurized first and isolated from the supply. The gripper was then actuated to perform the handshake (Fig. 3F, i and ii). Once inflated, the soft digits were squeezed powerfully to overpressurize them (Fig. 3Fiii). The finger with the soft valve at its tip let the air out, deflating further as the grip was tightened. Conversely, the other finger suffered irreversible damage because of the plastic deformation of the inflatable membranes at the tip (Fig. 3Fiv). Repeating the experiment showed that the behavior of the damaged finger was compromised: The tip of the finger was overinflated from the start, and the bending angle of the digit was reduced. A second squeeze caused the actuator to burst at the site of the damage (Fig. 3Fv), making it unresponsive, in contrast with the performance of the finger with the soft valve at its tip, which remained unaltered (Fig. 3Fvi).

Two-stage soft valve achieves endogenous control and fault isolation

EC soft valve characterization

One challenge that arises at the system level when using soft valves in FOM is knowing when to pressurize the control chamber because its premature actuation can lead to the isolation of the SIE from the supply. The delay required between the pressurization of the two

Downloaded from https://www.science.org at The Hong Kong University of Science and Technology (Guangzhou) on May 25, 2026

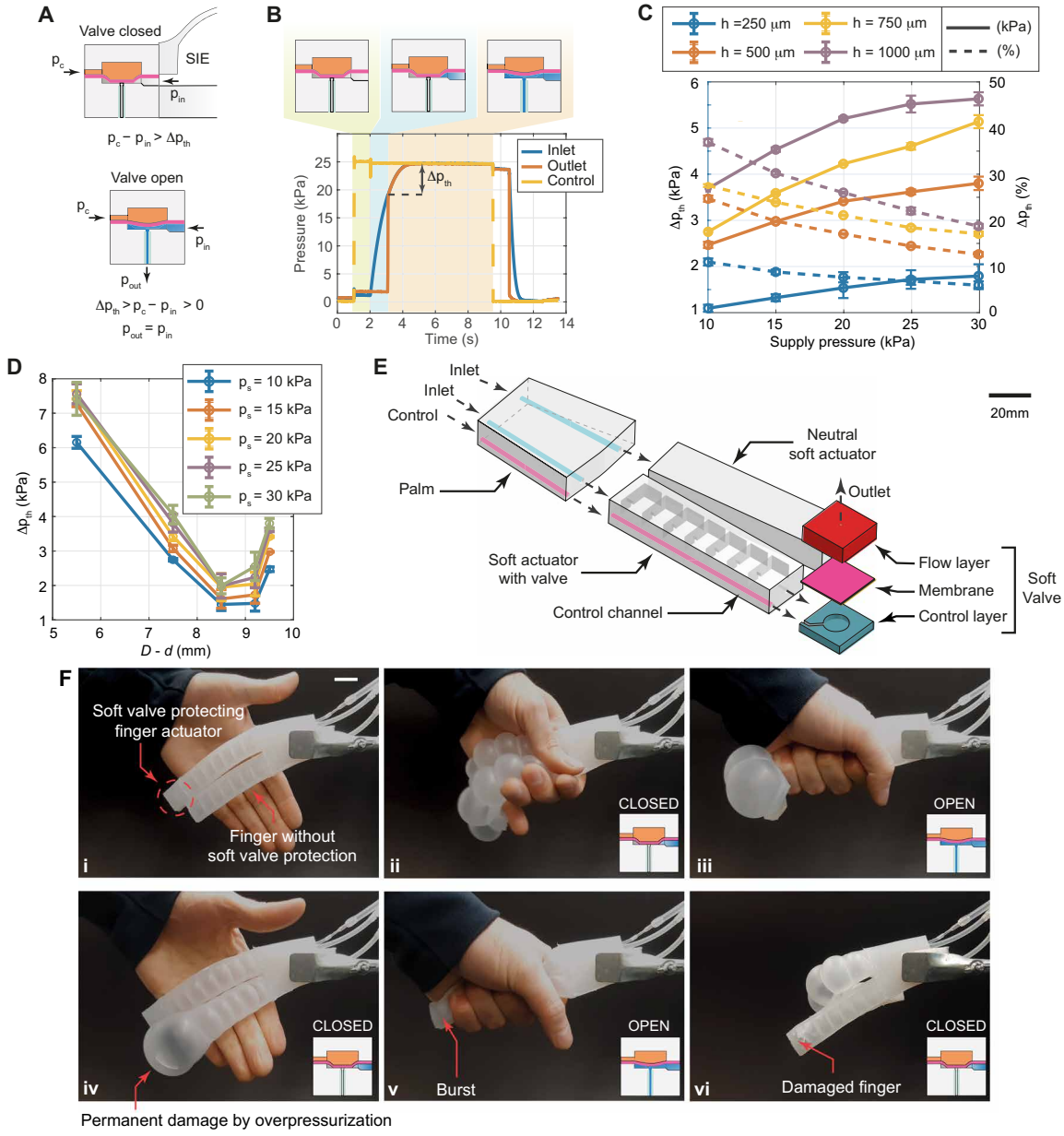

Fig. 3. ROM behavior characterization and demonstration. (**A**) Working principle of the valve's ROM. (**B**) Representative experiment demonstrating the working principle of the valve and its characterization ($D = 6$ mm, $d = 0.5$ mm, and $h = 500$ μm). (**C**) Effect of different membrane thicknesses with $D = 10$ mm and $d = 0.5$ mm on Δp_{th}. Error bars in plots indicate the average SD ($N = 15$) obtained in the trials [also in (**D**)]. For details on statistical analysis, refer to Materials and Methods. (D) The parameter $D - d$ was used as the metric to compare various geometries of the valve. The best performing one, a minimum of the curves, was obtained with a difference $D - d = 8.5$ mm. (**E**) Structure of the two-finger soft hand with all the relevant components and connections. (**F**) Demonstration showing the overpressurization protection capabilities of the ROM-configured soft valve. The scale bar in the figure represents 20 mm. Only the top finger was being protected by the soft valve. Upon inflation, the fingers were squeezed, causing irreparable damage to the unprotected finger (i to iv). The same finger then burst after a second run of the experiment (v), whereas the finger protected by the valve still performed the same as upon the first inflation (vi).

channels depends on multiple factors, such as the supply pressure level, overall SIE volume, geometry, and material properties. Extensive system characterization is required, and challenges remain when different SIEs share the same control line. To avoid these problems, two soft valves can be combined into a unit capable of endogenous control signal generation. This behavior is automatic and does not rely on external pressure sensors, valves, or controllers, thereby eliminating the need for an external control channel.

The EC soft valve was created by stacking two soft valves in a main stage at the bottom and in a delay stage at the top, operating at a single supply pressure level (Fig. 4A). The principle of operation is illustrated in Fig. 4B with an actuator volume of 1 liter. The SIE was

Downloaded from https://www.science.org at The Hong Kong University of Science and Technology (Guangzhou) on May 25, 2026

deflated, and both membranes started out in their relaxed states (both soft valves were open). Upon activation of the inlet channel ($t = 1.0$ s), the delay stage control chamber was pressurized immediately. Consequently, the top membrane deformed, closing the valve and initializing the delay stage in ROM. Meanwhile, the airflow passed through the FOM-configured main stage and reached the SIE, where the pressure started to increase. The increase in the main stage control pressure during this initial phase resulted from the slowly increasing outlet pressure, which deformed the main stage membrane upward, compressing the air trapped in the control chamber. Once the outlet pressure reached the correct threshold value, the delay stage opened, allowing the air to flow through and pressurize the control chamber of the main stage ($t \approx 7.5$ s). Henceforth, if a burst occurred, the delay stage autonomously turned to FOM because of the inversion of the pressure gradient, and the membrane switched, trapping the air present in the control chamber of the main stage. The main stage also switched, thus isolating the faulty SIE from the remainder of the system. A main stage with a small chamber diameter ($D = 6$ mm) and inlet diameter ($d = 0.5$ mm) was selected to obtain the fastest FOM behavior, whereas a larger chamber diameter ($D = 10$ mm) was used for the delay stage to improve the ROM behavior performance.

The delay stage, which starts in ROM, is key to achieving endogenous control because the control channel of the main stage is pressurized only once the pressure in the SIE reaches a sufficiently high level, independent of the SIE volume, geometry, or material. When voluntarily deflating the SIE, the soft valve did not impede the deflation because the control channel of the delay stage depressurized first. To confirm that the EC soft valve could be paired with SIEs of any volume and self-tune its own operation, valves were connected to a wide range of volumes, from 50 ml to 1.0 liter (fig. S8). The effect of the SIE volume on the self-tuned delay time, or the time it takes for the delay stage to open, Δt_d, between the initial pressurization of the inlet channel and the pressurization of the main stage control chamber is shown in Fig. 4C. This effect is evident, with the delay increasing almost linearly from approximately 260 ms to 6.0 s as the volume increased from 50 ml to 1.0 liter. Furthermore, the figure shows that an increase in the supply pressure increases the Δt_d and that the effect becomes more pronounced at larger volumes: A 42-ms difference was observed for a 50-ml volume between 10 and 20 kPa, whereas at 1.0 liter, the difference became 1.7 s. In contrast, the Δp_{th} needed for the delay stage to open was almost constant, independent of the volume: The maximum measured difference was less than 1.0 kPa between the smallest and largest volumes, with a supply pressure of 10 kPa. Last, the opening Δp_{th} measured across all volumes and supply pressure levels was consistent with the results obtained previously for the ROM-configured simple valve ($D = 10$ mm, $d = 0.5$ mm, and $h = 500$ μm). The automatic burst detection and isolation of the valve were tested by pairing it with ballooning actuators of two different sizes (fig. S9 and movie S3). The results obtained with the smaller of the two (12-mm diameter of a deflated membrane) are shown in Fig. 4D, where $\Delta t_d = 0.16$ s. The soft valve was able to fully isolate the burst that happened around $t = 6.5$ s. After the sudden depressurization of the outlet, the delay stage switched, isolating the main stage control chamber from the outlet (the yellow line in Fig. 4D decoupled from the red line after the burst). The main stage also closed, separating the inlet pressure, which remained equal to the supply pressure, from the outlet, which dropped to ambient pressure. As shown in Fig. 4D, the main stage control pressure after the burst stabilized at an intermediate pressure value between the supply and ambient pressures. This value depends on the expansion of the control chamber when the main stage switches and the depressurization caused by the air that escapes from the chamber before the delay stage has closed. Because the burst can be considered almost instantaneous, the value depends only on the supply pressure and specifics of the valve (internal geometry and material properties) (fig. S9).

Autonomous burst detection and isolation in a pneumatic soft crawler

The seamless integration of the EC valve in existing soft robots was demonstrated using a soft crawler manufactured from two bellows-type actuators. The actuators shared the same supply, as shown in Fig. 4E, and were inflated and deflated simultaneously. The crawling motion was enabled by the asymmetric friction provided by the feet, through the combination of its 7° inclination angle and the low-friction wiper insert. The valves were placed inside the empty volume of the actuators to achieve compactness and simplify the routing of the pneumatic channels.

The crawler was subjected to a pressure of 12.5 kPa for 5.5 s and then partially deflated for 1.2 s, which resulted in an actuation frequency of 0.15 Hz (Fig. 4F and movie S4). The partial deflation of the actuators decreased the crawling speed but was necessary to keep the internal channels of the EC valves pressurized. Using the aforementioned actuation sequence, the robot achieved an average crawling speed of 42 mm/min (Fig. 4F, i and ii). The front bellows actuator suddenly burst using a sharp blade, and the front EC valve was switched and isolated from the supply (Fig. 4Fiii). Because of the partial deflation technique, the pressure in the control chamber of the delay stage did not disappear, keeping the front actuator isolated, whereas the rear one kept being actuated. Therefore, the robot could continue crawling at a reduced speed of 21.4 mm/min (Fig. 4F, iv and v). No changes to the control sequence were required, and no sensors were present onboard, demonstrating the completely passive and autonomous nature of the approach. Last, the robot was submerged in water (Fig. 4Fvi) to demonstrate the absence of air bubbles originating from the burst actuator, further indicating its successful isolation.

DISCUSSION

Soft valves in soft robotic designs have demonstrated the possibility of controlling the behavior of robots without any onboard electronics (*29*, *31*). In addition, they offer the possibility of low-cost manufacturing and tailored performance as well as the potential for monolithic integration, paving the way for fully soft robots. Thus far, very few studies have examined the possibility of using these components for anything besides logic gates in control units. In this study, we presented a multimodal soft valve that endowed resilience to soft robots through an embodied, passive, and autonomous approach without controller interventions. The valve could be easily integrated into existing pneumatic soft robotic designs, with small alterations required during the manufacturing process.

Inspired by the innate mechanisms observed in biological systems, this work explored the possibility of using soft valves to preemptively avoid faults or limit their adverse effects in soft robots, thus providing continuous operation and extended life span. In FOM, the soft valve can autonomously detect and isolate bursts in pneumatic SIEs by reacting to the sudden drop in pressure created by the burst itself. The experimental characterization highlighted the effect of critical design parameters, such as the geometry of the

Downloaded from https://www.science.org at The Hong Kong University of Science and Technology (Guangzhou) on May 25, 2026

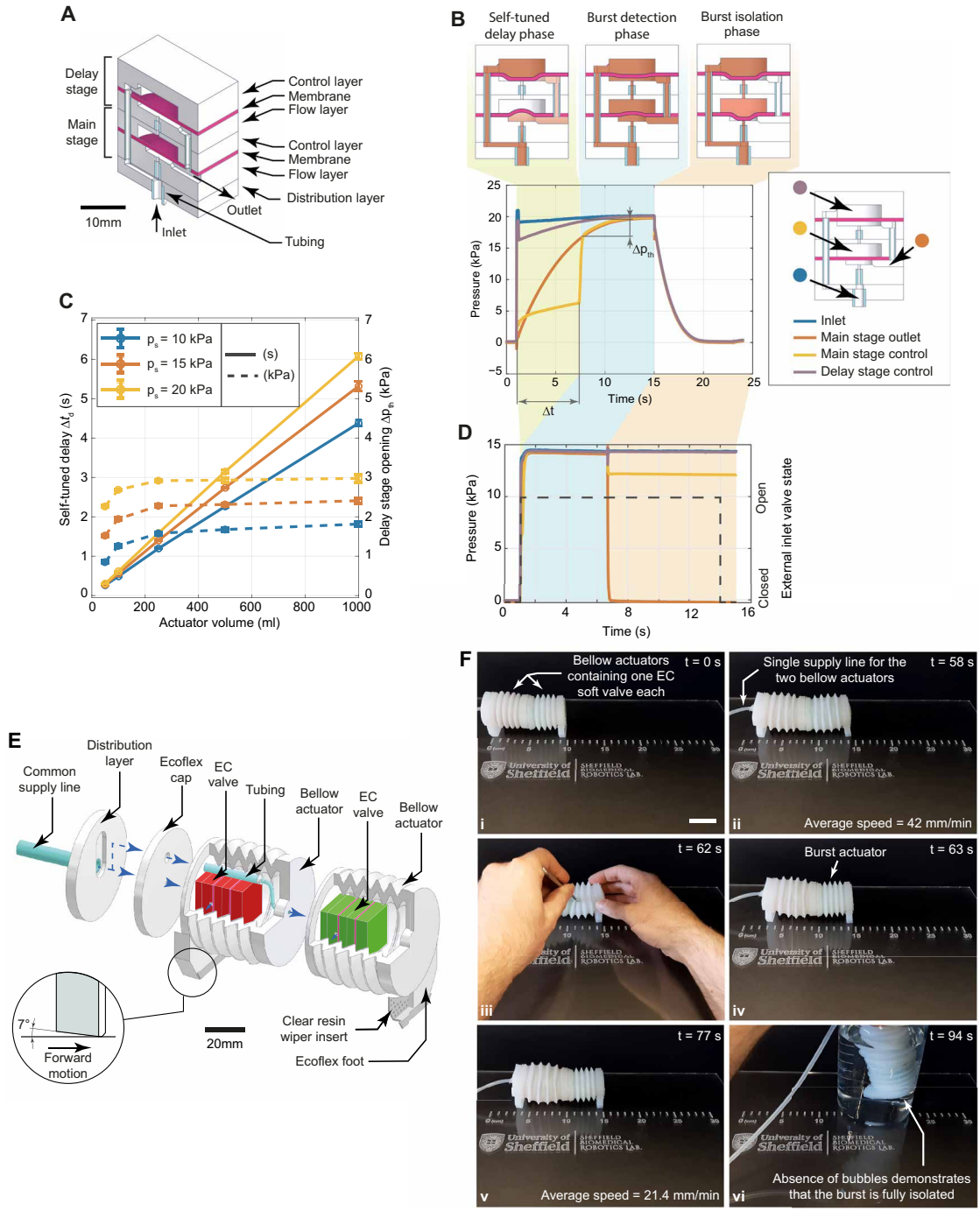

Fig. 4. EC soft valve characterization and burst isolation demonstration in a soft crawler. (**A**) Internal structure of the two-stage EC soft valve. The main stage at the bottom ($D = 6$ mm, $d = 0.5$ mm, and $h = 500$ μm) is internally connected to the delay stage at the top ($D = 10$ mm, $d = 0.5$ mm, and $h = 500$ μm). The EC valve can generate its own control signal thanks to the joint action of the two valves, which enables self-tuning operation. (**B**) Representative experiment used to capture the behavior of the valve in terms of Δp_{th} and Δt_d with an actuator volume of 1 liter. (**C**) Δp_{th} and Δt_d were obtained by varying the supply pressure and the actuator volume between 50 ml and 1.0 liter. Error bars represent average SDs ($N = 15$). Δt_d increased linearly with the volume from 260 ms to 6.0 s, proving the self-tuning capability of the soft valve. After the ROM characterization, for the same volume, Δp_{th} increased with higher supply pressures. When changing the volume at a constant p_s, Δp_{th} remained almost constant, proving that Δt_d is mostly affected by the SIE volume. (**D**) Burst isolation using the two-stage EC valve. A ballooning actuator (see fig. S9 for details) was used for the experiment. The threshold pressure needed to open the delay stage was reached in less than 200 ms, and the valve successfully isolated the burst ($t = 8$ s). (**E**) Internal structure of the soft crawler integrating two EC soft valves. (**F**) The soft crawler achieved an average moving speed of 42 mm/min with a supply pressure of 12.5 kPa (i and ii). The scale bar represents 40 mm. A sharp blade was used to cut into the side of the front actuator, bursting it (iii). The burst front actuator was kept isolated by the corresponding EC valve, whereas the back one operated normally (iv and v). To prove the successful isolation of the burst, the robot was submerged in water while still being actuated, and no air bubbles were observed (vi).

Downloaded from https://www.science.org at The Hong Kong University of Science and Technology (Guangzhou) on May 25, 2026

inlet channel, on the switching time of the valve, leading to a design that could consistently isolate burst SIEs in as fast as 21 ms, which is 12 ms faster than the average duration of a human blink (*47*). This capability makes it possible to fabricate soft robots that can maintain their functionality in case one or more SIEs burst, with only one common inlet channel, substantially reducing the need for external hardware and the complexity of the control logic. In addition, a partial deflation technique, similar to that used for the soft crawler, can be used to operate the soft robot while keeping the faulty fingers fully isolated. Swapping the inlet and outlet channels activates the ROM behavior, which can be used to protect against accidental overpressurization. The importance of this capability was demonstrated in a human-robot interaction application. During the experiment, one of the soft actuators plastically deformed before bursting, leading to irreparable damage. This type of damage irrecoverably alters the performance of the actuator, with overinflation of the damaged section; however, it would not be detected by material self-healing approaches because the continuity of the material matrix was not compromised. Therefore, the ROM-configured valve enables a preemptive type of resilience, as opposed to the more common ex post one. The threshold value that toggles the valve can be tuned to specific needs by varying the control pressure and geometrical design parameters.

A common challenge in soft robot control stems from the hyperelasticity of soft materials, which leads to accentuated nonlinear behavior upon repeated inflation. Successful control requires prior knowledge of SIEs, achieved either through numerical modeling or extensive experimental training (*48*–*50*). This limits the usability of the valve in FOM, whereas the ROM behavior is not affected because the control signal is always present. By pairing the FOM and ROM valve configurations, we demonstrated the possibility of creating a soft valve that generates its own control signal using direct feedback from the SIE it is paired with. Consequently, despite having only one inlet and one outlet port, the valve could achieve autonomous burst detection and isolation, irrespective of the nonlinear behavior or size of the SIE. For this to occur, the valve's delay stage automatically swaps from ROM to FOM when a burst occurs, which further highlights the importance of the valve's multimodality. The absence of an external control line makes this pneumatic component a truly self-contained solution for soft robotic resilience, increasing its usability as a drop-in solution in many soft robotic applications. Despite only one elastomer being tested in this study, the working principles of the soft valves rely on fluid dynamics rather than material properties. Stiffer materials can therefore be used provided that the supply pressure is increased, which would be justified by the increased stiffness of the soft actuators the valves are paired to.

Although full integration of the soft valves into the body of soft robots was demonstrated in this study, the fabrication currently requires several manual steps that slow down manufacturing and limit accuracy and repeatability. With the increasing availability of soft 3D-printing materials, additive manufacturing techniques can provide solutions, leading to possible monolithic fabrication (*29*–*31*). The design could be fully replicated with multimaterial printers capable of soluble supports. Bridging techniques could also be used, where available, to avoid the use of support material together. A second advantage of additive manufacturing techniques entails further miniaturization of the design, which might be required to enable the full potential of a distributed fault-resilience approach at larger scales. One drawback of miniaturization may be the reduction in the maximum flow rates through fluidic components, which leads to increased delays and consequent negative effects on system dynamics. However, with thoughtful design, we believe that the local distributed control approach presented in this study may still be beneficial in reducing the reaction times associated with long and narrow supply lines, which are characteristic of complex microfluidic systems. In such systems, minimizing the physical distance between logic and actuation, as demonstrated in this work, is crucial for achieving the fast reaction times required for critical applications such as burst detection and isolation.

The soft valve presented in this study can form a unifying platform for resilient soft robots by integrating passive preemptive fault isolation with material healing techniques. Some of the current limitations of approaches based on self-healing materials include time to recovery and inactivity during healing. The FOM-configured soft valve responds to these limitations by providing deflation and isolation of the faulty actuator. Pairing these technologies would result in the creation of soft robots that can operate, whereas their bodies heal from faults. The approach represents an evolution in the fluidic control and resilience of soft robots, a first step toward transforming the common centralized architecture (with one fluidic controller managing the entire robot) into a distributed one (where local control units autonomously manage the resilience of each SIE). The valves provide hard-coded primitive responses to the system, similar to the instinctive reactions humans experience when responding to threats, independent of the higher-level control logic, meant to protect and preserve the welfare of the system as a whole. Building on responsive mechanisms, more complex systems can be developed in which units can exchange signals and transfer information using fluidics as a medium, expanding on the paradigm presented in (*51*). The inclusion of distributed fault signaling (*21*, *52*) could lead to the possibility of performing system-level behavior changes to compensate for the faulty section of the robot, either temporarily, while the system is healing, or permanently, further improving the overall resilience. In the long term, these approaches, extended by advancements in biodegradable self-healing materials (*19*, *20*, *53*), are expected to enable the creation of robots that can maximize their life expectancy, recover from multiple faults while carrying out various tasks, and ultimately degrade and provide resources for other organisms or robots.

MATERIALS AND METHODS

Fabrication of the valves

Single valve fabrication

The valve consists of three layers molded out of Ecoflex 00-50 (1:1 ratio of parts A and B, mixed for 3 min in an ARE-249 mixer by Thinky). All molds were printed in clear resin using 50-μm resolution on a Form2 printer. The tubing was cut to length and inserted into the inlet channel area, stopping approximately 1 mm before entering the flow layer chamber. Therefore, the membrane interfaces with a smooth continuous surface when deformed, maximizing the sealing potential. The molds were prepared with Ease Release 200, and the silicone was cast and cured at 20°C for 4 hours. Once solid, the flow and control layers were unmolded, whereas the membrane was left untouched to avoid wrinkling. Sil-Poxy glue was uniformly applied to the surface of the flow layer, which was then pressed onto the membrane. Last, the pair was bonded to the control layer. The glue was applied to the control layer and not the membrane directly

Downloaded from https://www.science.org at The Hong Kong University of Science and Technology (Guangzhou) on May 25, 2026

to avoid application of adhesive on areas that do not require it, which could locally alter the mechanical properties of the membrane.

Two-stage self-tuning valve

As shown in fig. S10, layers 2 and 3 as well as layers 4 and 5 were glued together after molding. Once the glue was set, a syringe needle (external diameter of 1 mm) was passed through the central holes of components 4 and 5 to ensure that the channel was glue free. Then, the pairs were joined by gluing layers 3 and 4 together. A wide needle was run through the side channels, cutting the membrane that obstructed them, and the 3D-printed elements 8 and 9 (printed in clear resin on a Form3 printer) were inserted into these. Last, layers 1 and 7 were added to the stack, completing the fabrication process. The main stage had the following geometric parameters: $D = 6$ mm, $d = 0.5$ mm, and $h = 500$ μm. For the delay stage, a valve with $D = 6$ mm, $d = 0.5$ mm, and $h = 500$ μm was used.

Characterization of the valves

An Arduino Nano paired with a custom-designed printed circuit board was used to control the pneumatic hardware during the characterization of the soft valves and for the demo applications. In addition, all sensors were sampled at 10 kHz using a custom-designed data acquisition system capable of simultaneous sampling on eight channels at a 16-bit resolution. The remaining hardware included five 12-V dc solenoid valves, five pressure sensors (Honeywell AVX005PGAA5), a volumetric flow sensor (Renesas FS1012-1100-NG), a peristaltic pump, two 5.0-liter accumulators, a flow regulator, a 50-ml syringe, tubing (4-mm inner diameter), and Tee tubes. For a detailed description of the hardware required for each experiment, please refer to figs. S11 to S14. In the figures, V1, V2, V3, V4, and V5 refer to the solenoid valves.

FOM characterization experiments

As shown in fig. S11, valve V1 controlled the inlet to the flow layer of the soft valve, V2 controlled the outlet, and V3 and V4 managed the inlet and outlet of the control channel of the soft valve, respectively. A flow sensor was placed between the soft valve and V2 to record the airflow out of the soft valve. The pressure in the accumulator was stabilized at the target pressure, and the pump was switched off to enable accurate pressure measurements. There were four phases in the experiment: The inlet channel was pressurized first (left flow rate spike in Fig. 2B), followed by the control channel. After 2.0 s, V2 was opened to simulate a burst, connecting the main supply to the atmosphere. After a brief initial air discharge, the membrane inside the soft valve blocked the flow and isolated the main supply. This discharge, which corresponds to the middle spike in the flow sensor signal, was used to evaluate the response time of the valve. The time, Δt, required for the valve to isolate the burst was defined by the intersection between the flow rate (Fig. 2B) and the threshold line. The threshold value was set to 10% higher than the output noise of the flow sensor at rest. The fourth and final step was resetting the pneumatic circuit by depressurizing the channels (right flow rate spike).

Eight designs of the soft valve were manufactured (three samples per design) and tested. Four different membrane thicknesses were produced: 250, 500, 750, and 1000 μm ($d = 0.5$ mm and $D = 10$ mm). d was varied from 0.5 to 0.8 to 1.5 mm (constant membrane thickness of 500 μm, $D = 10$ mm), whereas D was changed from 6 to 8 to 10 mm (constant membrane thickness of 500 μm, $d = 0.5$ mm). In addition, the supply pressure level p_s was varied from 10 to 30 kPa. The spikes visible in the flow rate data refer to the initial pressurization of the circuit, simulated burst, and reset of the pneumatic circuit before the next experiment.

ROM characterization experiments

As displayed in fig. S12, valve V1 managed the inlet to the soft valve, V2 managed the outlet, V3 allowed the pressurization of the control channel, and V4 controlled its deflation. Similar to the FOM experiments, the pressure was stabilized in the tank and the pump was switched off. A 35-ml volume, together with a flow regulator, was used to slow down the pressurization of the inlet channel and allow more precise measurements. These can be considered as the SIE connected to the soft valve. The same membrane thicknesses and internal geometries were used as described previously. Each experimental trial consisted of three phases. Valve V3 was opened to pressurize the control channel. V1 was opened 1.0 s later, allowing the air to enter the main channel of the soft valve. The valve opened when the pressure at the inlet of the soft valve reached a threshold value dependent on the control pressure, and the outlet channel was pressurized. At that instant, the difference between the control and inlet pressures determined the opening Δp_{th} for the valve in those conditions. The final phase comprised a circuit reset for the next trial. The main inlet valve was closed, the control channel was depressurized, and the outlet valve was opened for 3.0 s.

EC valve characterization

Only two valves were required to characterize the EC soft valve: V1 controlled the main inlet, whereas V2 controlled the outlet (fig. S13). A 5.0-liter glass container served as the varying SIE volume. Water was used to precisely regulate the air volume within it in the range of 50 ml to 1.0 liter. Three soft valve samples were manufactured and tested at three different supply pressures (10, 15, and 20 kPa). The actuator volume was varied from 50 ml to 1.0 liter to cover a wide range of soft robotics applications and to better highlight the self-tuning capability of the soft valve. Five trials were performed for each supply pressure level and actuator volume. During each experiment, valve V1 was kept open for a sufficiently long time for the actuator volume to reach the supply pressure level. V1 was then closed, and V2 was opened to depressurize the actuator and soft valve, resetting the circuit for the next run. For the burst detection and isolation experiments, the outlet reservoir and valve V2 were replaced by the ballooning actuators (figs. S9 and S14).

Fabrication and control of the soft robots

The fabrication process for each robot is detailed in Supplementary Methods, together with a description of the hardware needed for each demonstration and the corresponding pneumatic circuit.

Statistical analysis

Each data point in the charts represents the average of 15 trials. For each experiment, three valve samples were tested and five trials were conducted at constant conditions. The average SDs were computed using the equation

$$SD = \sqrt{\frac{1}{3}\left({SD_1}^2 + {SD_2}^2 + {SD_3}^2 \right)} \quad (3)$$

where SD_1, SD_2, and SD_3 represent the SDs obtained for each sample. When evaluating whether the membrane thickness had a statistically significant effect on the FOM switching time, separate one-way ANOVA tests were conducted, and the five resulting P values were then averaged to get the final one (table S1). For each supply pressure

Downloaded from https://www.science.org at The Hong Kong University of Science and Technology (Guangzhou) on May 25, 2026

value, four groups were compared, one for each membrane thickness, and each group contained data from all three samples and all five repetitions (15 data points in total in each group).

Supplementary Materials

The PDF file includes:
Methods
Figs. S1 to S18
Table S1

Other Supplementary Material for this manuscript includes the following:
Movies S1 to S4

REFERENCES AND NOTES

1. C. S. X. Ng, G. Z. Lum, Untethered soft robots for future planetary explorations? *Adv. Intell. Syst.* **5**, 2021–2024 (2023).
2. C. Majidi, Soft-matter engineering for soft robotics. *Adv. Mater. Technol.* **4**, 1800477 (2019).
3. P. Polygerinos, N. Correll, S. A. Morin, B. Mosadegh, C. D. Onal, K. Petersen, M. Cianchetti, M. T. Tolley, R. F. Shepherd, Soft robotics: Review of fluid-driven intrinsically soft devices; manufacturing, sensing, control, and applications in human-robot interaction. *Adv. Eng. Mater.* **19**, 1700016 (2017).
4. E. T. Roche, M. A. Horvath, I. Wamala, A. Alazmani, S. E. Song, W. Whyte, Z. Machaidze, C. J. Payne, J. C. Weaver, G. Fishbein, J. Kuebler, N. V. Vasilyev, D. J. Mooney, F. A. Pigula, C. J. Walsh, Soft robotic sleeve supports heart function. *Sci. Transl. Med.* **9**, eaaf3925 (2017).
5. Y. Zhang, P. Li, J. Quan, L. Li, G. Zhang, D. Zhou, Progress, challenges, and prospects of soft robotics for space applications. *Adv. Intell. Syst.* **5**, 2200071 (2023).
6. E. Perez-Guagnelli, J. Jones, A. H. Tokel, N. Herzig, B. Jones, S. Miyashita, D. D. Damian, Characterization, simulation and control of a soft helical pneumatic implantable robot for tissue regeneration. *IEEE Trans. Med. Robot. Bionics.* **2**, 94–103 (2020).
7. D. Rus, M. T. Tolley, Design, fabrication and control of soft robots. *Nature* **521**, 467–475 (2015).
8. S. Terryn, J. Brancart, D. Lefeber, G. Van Assche, B. Vanderborght, Self-healing soft pneumatic robots. *Sci. Robot.* **2**, eaan4268 (2017).
9. K. Man, A. Damasio, Homeostasis and soft robotics in the design of feeling machines. *Nat. Mach. Intell.* **1**, 446–452 (2019).
10. T. Zhang, W. Zhang, M. M. Gupta, Resilient robots: Concept, review, and future directions. *Robotics* **6**, 22–36 (2017).
11. J. Bongard, V. Zykov, H. Lipson, Resilient machines through continuous self-modeling. *Science* **314**, 1118–1121 (2006).
12. A. Cully, J. Clune, D. Tarapore, J. B. Mouret, Robots that can adapt like animals. *Nature* **521**, 503–507 (2015).
13. K. Gilpin, D. Rus, Modular robot systems. *IEEE Robot. Autom. Mag.* **17**, 38–55 (2010).
14. A. Brunete, A. Ranganath, S. Segovia, J. P. de Frutos, M. Hernando, E. Gambao, Current trends in reconfigurable modular robots design. *Int. J. Adv. Robot. Syst.* **14**, 1729881417710457 (2017).
15. S. Li, R. Batra, D. Brown, H. D. Chang, N. Ranganathan, C. Hoberman, D. Rus, H. Lipson, Particle robotics based on statistical mechanics of loosely coupled components. *Nature* **567**, 361–365 (2019).
16. R. Adam Bilodeau, R. K. Kramer, Self-healing and damage resilience for soft robotics: A review. *Front. Robot. AI.* **4**, 48 (2017).
17. M. J. Ford, C. P. Ambulo, T. A. Kent, E. J. Markvicka, C. Pan, J. Malen, T. H. Ware, C. Majidi, A multifunctional shape-morphing elastomer with liquid metal inclusions. *Proc. Natl. Acad. Sci. U.S.A.* **116**, 21438–21444 (2019).
18. C. E. Diesendruck, N. R. Sottos, J. S. Moore, S. R. White, Biomimetic self-healing. *Angew. Chemie - Int. Ed.* **54**, 10428–10447 (2015).
19. M. Baumgartner, F. Hartmann, M. Drack, D. Preninger, D. Wirthl, R. Gerstmayr, L. Lehner, G. Mao, R. Pruckner, S. Demchyshyn, L. Reiter, M. Strobel, T. Stockinger, D. Schiller, S. Kimeswenger, F. Greibich, G. Buchberger, E. Bradt, S. Hild, S. Bauer, M. Kaltenbrunner, Resilient yet entirely degradable gelatin-based biogels for soft robots and electronics. *Nat. Mater.* **19**, 1102–1109 (2020).
20. Z. Wei, J. H. Yang, Z. Q. Liu, F. Xu, J. X. Zhou, M. Zrínyi, Y. Osada, Y. M. Chen, Novel biocompatible polysaccharide-based self-healing hydrogel. *Adv. Funct. Mater.* **25**, 1352–1359 (2015).
21. H. Wang, S. Terryn, Z. Wang, G. Van Assche, F. Iida, B. Vanderborght, Self-regulated self-healing robotic gripper for resilient and adaptive grasping. *Adv. Intell. Syst.* **5**, 2300223 (2023).
22. T. J. Koh, L. A. DiPietro, Inflammation and wound healing: The role of the macrophage. *Expert Rev. Mol. Med.* **13**, e23 (2011).
23. O. Speck, T. Speck, An overview of bioinspired and biomimetic self-repairing materials. *Biomimetics* **4**, 26 (2019).
24. S. A. Eming, P. Martin, M. Tomic-Canic, Wound repair and regeneration: Mechanisms, signaling, and translation. *Sci. Transl. Med.* **6**, 265sr6 (2014).
25. E. C. Jensen, W. H. Grover, R. A. Mathies, Micropneumatic digital logic structures for integrated microdevice computation and control. *J. Microelectromech. Syst.* **16**, 1378–1385 (2007).
26. B. Mosadegh, T. Bersano-Begey, J. Y. Park, M. A. Burns, S. Takayama, Next-generation integrated microfluidic circuits. *Lab Chip* **11**, 2813–2818 (2011).
27. M. Rhee, M. A. Burns, Microfluidic pneumatic logic circuits and digital pneumatic microprocessors for integrated microfluidic systems. *Lab Chip* **9**, 3131–3143 (2009).
28. P. N. Duncan, S. Ahrar, E. E. Hui, Scaling of pneumatic digital logic circuits. *Lab Chip* **15**, 1360–1365 (2015).
29. M. Wehner, R. L. Truby, D. J. Fitzgerald, B. Mosadegh, G. M. Whitesides, J. A. Lewis, R. J. Wood, An integrated design and fabrication strategy for entirely soft, autonomous robots. *Nature* **536**, 451–455 (2016).
30. S. Wang, L. He, P. Maiolino, A modular approach to design multi-channel bistable valves for integrated pneumatically-driven soft robots via 3D-printing. *IEEE Robot. Autom. Lett.* **7**, 3412–3418 (2022).
31. Y. Zhai, A. De Boer, J. Yan, B. Shih, M. Faber, J. Speros, R. Gupta, M. T. Tolley, Desktop fabrication of monolithic soft robotic devices with embedded fluidic control circuits. *Sci. Robot.* **8**, eadg3792 (2023).
32. K. L. Dorsey, Electronics-free soft robot has a nice ring to it. *Sci. Robot.* **7**, eabn6551 (2022).
33. V. Cacucciolo, J. Shintake, Y. Kuwajima, S. Maeda, D. Floreano, H. Shea, Stretchable pumps for soft machines. *Nature* **572**, 516–519 (2019).
34. W. Tang, C. Zhang, Y. Zhong, P. Zhu, Y. Hu, Z. Jiao, X. Wei, G. Lu, J. Wang, Y. Liang, Y. Lin, W. Wang, H. Yang, J. Zou, Customizing a self-healing soft pump for robot. *Nat. Commun.* **12**, 2247 (2021).
35. S. Xu, C. M. Nunez, M. Souri, R. J. Wood, A compact DEA-based soft peristaltic pump for power and control of fluidic robots. *Sci. Robot.* **8**, eadd4649 (2023).
36. F. Perdigones, A. Luque, J. M. Quero, Correspondence between electronics and fluids in MEMS: Designing microfluidic systems using electronics. *IEEE Ind. Electron. Mag.* **8**, 6–17 (2014).
37. S. Song, S. Joshi, J. Paik, CMOS-inspired complementary fluidic circuits for soft robots. *Adv. Sci.* **8**, 2100924 (2021).
38. J. Teichmann, P. Auth, S. Conrad, T. Speck, F. J. Tauber, An insect-inspired soft robot controlled by soft valves, in *Biomimetic and Biohybrid Systems (Living Machines 2023)*, F. Meder, A. Hunt, L. Margheri, A. Mura, B. Mazzolai, Eds., vol. 14157 of *Lecture Notes in Computer Science* (Springer, 2023), pp. 428–441.
39. P. Rothemund, A. Ainla, L. Belding, D. J. Preston, S. Kurihara, Z. Suo, G. M. Whitesides, A soft, bistable valve for autonomous control of soft actuators. *Sci. Robot.* **3**, eaar7986 (2018).
40. D. J. Preston, H. J. Jiang, V. Sanchez, P. Rothemund, J. Rawson, M. P. Nemitz, W. K. Lee, Z. Suo, C. J. Walsh, G. M. Whitesides, A soft ring oscillator. *Sci. Robot.* **4**, eaaw5496 (2019).
41. W. K. Lee, D. J. Preston, M. P. Nemitz, A. Nagarkar, A. K. MacKeith, B. Gorissen, N. Vasios, V. Sanchez, K. Bertoldi, L. Mahadevan, G. M. Whitesides, A buckling-sheet ring oscillator for electronics-free, multimodal locomotion. *Sci. Robot.* **7**, eabg5812 (2022).
42. D. Drotman, S. Jadhav, D. Sharp, C. Chan, M. T. Tolley, Electronics-free pneumatic circuits for controlling soft-legged robots. *Sci. Robot.* **6**, eaay2627 (2021).
43. M. Wehner, M. T. Tolley, Y. Mengüç, Y. L. Park, A. Mozeika, Y. Ding, C. Onal, R. F. Shepherd, G. M. Whitesides, R. J. Wood, Pneumatic energy sources for autonomous and wearable soft robotics. *Soft Robot.* **1**, 263–274 (2014).
44. M. Pontin, S. Miyashita, D. D. Damian, Development and characterization of a soft valve for automatic fault isolation in inflatable soft robots, in *2022 IEEE 5th International Conference on Soft Robotics (RoboSoft)* (IEEE, 2022), pp. 62–67.
45. C. Bosio, D. Zrinscak, C. Laschi, M. Cianchetti, Soft mini fuse valve for resilient fluidically-actuated robots. *IEEE Robot. Autom. Lett.* **8**, 2716–2723 (2023).
46. R. F. Shepherd, F. Ilievski, W. Choi, S. A. Morin, A. A. Stokes, A. D. Mazzeo, X. Chen, M. Wang, G. M. Whitesides, Multigait soft robot. *Proc. Natl. Acad. Sci. U.S.A.* **108**, 20400–20403 (2011).
47. K. A. Kwon, R. J. Shipley, M. Edirisinghe, D. G. Ezra, G. Rose, S. M. Best, R. E. Cameron, High-speed camera characterization of voluntary eye blinking kinematics. *J. R. Soc. Interface* **10**, 20130227 (2013).
48. P. Schegg, C. Duriez, Review on generic methods for mechanical modeling, simulation and control of soft robots. *PLOS ONE* **17**, e0251059 (2022).
49. G. Mengaldo, F. Renda, S. L. Brunton, M. Bächer, M. Calisti, C. Duriez, G. S. Chirikjian, C. Laschi, A concise guide to modelling the physics of embodied intelligence in soft robotics. *Nat. Rev. Phys.* **4**, 595–610 (2022).
50. M. Grube, J. C. Wieck, R. Seifried, Comparison of modern control methods for soft robots. *Sensors (Basel)* **22**, 9464 (2022).
51. C. A. Aubin, S. Choudhury, R. Jerch, L. A. Archer, J. H. Pikul, R. F. Shepherd, Electrolytic vascular systems for energy-dense robots. *Nature* **571**, 51–57 (2019).
52. S. K. Tabrizian, F. Sahraeeazartamar, J. Brancart, E. Roels, P. Ferrentino, J. Legrand, G. Van Assche, B. Vanderborght, S. Terryn, A healable resistive heater as a stimuli-providing system in self-healing soft robots. *IEEE Robot. Autom. Lett.* **7**, 4574–4581 (2022).

Downloaded from https://www.science.org at The Hong Kong University of Science and Technology (Guangzhou) on May 25, 2026

53. A. Costa Cornellà, S. K. Tabrizian, P. Ferrentino, E. Roels, S. Terryn, B. Vanderborght, G. Van Assche, J. Brancart, Self-healing, recyclable, and degradable castor oil-based elastomers for sustainable soft robotics. *ACS Sustain. Chem. Eng.* **11**, 3437–3450 (2023).

Acknowledgments: We thank S. Miyashita for valuable discussions and R. Gross and S. Dogramadzi for reviewing our manuscript. We thank J. Jones, F. Forbes, K. Esendag, M. HA Mahmoud, and J. Liu for input on the manuscript. For the purpose of open access, the authors have applied a Creative Commons Attribution (CC BY) license to any Author Accepted Manuscript version arising. **Funding:** This work was supported by the Engineering and Physical Science Research Council DTP PhD Scholarship (to M.P.) and Engineering and Physical Science Research Council EP/X017486/1 (to D.D.). **Author contributions:** Conceptualization: M.P. and D.D. Methodology: M.P. and D.D. Investigation: M.P. Visualization: M.P. and D.D. Funding acquisition: M.P. and D.D. Project administration: M.P. and D.D. Supervision: D.D. Writing—original draft: M.P. and D.D. Writing—review and editing: M.P. and D.D. **Competing interests:** The authors declare that they have no competing interests. **Data and materials availability:** All (other) data needed to evaluate the conclusions in the paper are present in the paper or the Supplementary Materials. The data for this study have been deposited in the database at DOI https://zenodo.org/records/11949581.

Submitted 22 September 2023
Accepted 27 June 2024
Published 24 July 2024
10.1126/scirobotics.adk9978

Downloaded from https://www.science.org at The Hong Kong University of Science and Technology (Guangzhou) on May 25, 2026

Science Robotics

Multimodal soft valve enables physical responsiveness for preemptive resilience of soft robots

Marco Pontin and Dana D. Damian

Sci. Robot. **9** (92), eadk9978. DOI: 10.1126/scirobotics.adk9978

Editor's summary

Fluidic soft robots are vulnerable to failure from overpressurization and damage that leads to sudden loss of pressurization. To give these robots more resilience and extend their lifetimes, Pontin and Damian developed a multimodal pneumatic soft valve designed to isolate damage and avoid catastrophic failure. The valve passively reacts to pressure differences triggered by faults. In the forward operating mode, the valve can detect a burst and autonomously isolate the damaged section, maintaining pressure in the other parts of the robot. In the reverse operating mode, the valve can detect overpressurization and release air to prevent irreversible damage. The valve capabilities were demonstrated in a five-finger soft gripper, a two-finger soft hand, and a soft crawler that remained operational after damage. —Melisa Yashinski

View the article online

https://www.science.org/doi/10.1126/scirobotics.adk9978

Permissions

https://www.science.org/help/reprints-and-permissions

Use of this article is subject to the Terms of service

Science Robotics (ISSN 2470-9476) is published by the American Association for the Advancement of Science. 1200 New York Avenue NW, Washington, DC 20005. The title *Science Robotics* is a registered trademark of AAAS.

Copyright © 2024 The Authors, some rights reserved; exclusive licensee American Association for the Advancement of Science. No claim to original U.S. Government Works

Downloaded from https://www.science.org at The Hong Kong University of Science and Technology (Guangzhou) on May 25, 2026